Nano-Heterostructures Hot Paper

DOI: 10.1002/anie.201310513

A 1D/2D Helical CdS/$ZnIn_2S_4$ Nano-Heterostructure**

*Biao Xu, Peilei He, Huiling Liu, Pengpeng Wang, Gang Zhou, and Xun Wang**

Abstract: *Multidimensional nano-heterostructures (NHSs) that have unique dimensionality-dependent integrative and synergic effects are intriguing but still underdeveloped. Here, we report the first helical 1D/2D epitaxial NHS between CdS and $ZnIn_2S_4$. Experimental and theoretical studies reveal that the mismatches in lattice and dangling bonds between 1D and 2D units govern the growth procedure. The resulting well-defined interface induces the delocalized interface states, thus facilitate the charge transfer and enhance the performance in the photoelectrochemical cells. We foresee that the mechanistic insights gained and the electronic structures revealed would inspire the design of more complex 1D/2D NHSs with outstanding functionalities.*

Recently low-dimensional materials have drawn continuous attention, owing to their unique properties arising from the diverse ways that electrons behave in different dimensions.[1] Among them, 1D systems[2–8] have been regarded as the smallest-dimension structures for efficient transport of electrons and optical excitation. Whereas 2D materials such as graphene[9,10] and layered metal chalcogenides[11,12] demonstrate excellent properties owing to the confinement of electrons in their unique atomic layers. To fully integrate the above-mentioned merits and mitigate the drawbacks of the single units, such as the low surface area of 1D nanowires and the tendency of 2D nanosheets towards restacking, the concept of 1D/2D NHSs was proposed,[13] yet remains quite new. The interface between these two segments might introduce the engineering in the electronic states that produce new attributes that are different from the single components.[14]

Up to now, little effort has been concentrated on the growth of 2D nanosheets on 1D nanomaterials.[15–18] However, the as-grown nanosheets have either a random orientation or a thickness larger than several lattices. The epitaxial growth of a 2D nanosheet through its lateral dangling bonds onto a 1D nanowire is expected to allow the exposure of almost its entire surface. In 2D materials, the atomic thickness would introduce unique electronic properties that differed from the bulk due to the confinement effect.[1,11,12] However, the epitaxy of 2D nanosheets with atomic thickness on 1D nanowires still remains unknown. The slow progress in 1D/2D NHSs might stem from the combination of different growth modes of 1D and 2D nanostructures in one synthetic system, and the judicious control to establish the oriented 1D/2D interface.[13] To promote this field in a systematic way, it is necessary to gain insight into the formation and bonding of the 1D/2D interface. Apart from controlled synthesis, there are urgent demands in the in-depth investigation of the modulation in electronic states by the 1D/2D interface, which govern the enhanced performance. These two aspects would thrust the rational design of the 1D/2D NHSs and the optimization of their functionalities, but still set a great challenge.

Inspired by the progress in 1D nanomaterials for solar energy conversion,[19,20] and the recent booming of 2D nanomaterials in this field,[21–22] we herein report our attempts to explore the area of 1D/2D NHSs for photo electrochemical cells (PECs). CdS and $ZnIn_2S_4$, which serve as efficient photocatalysts,[23,24] were chosen as the building blocks because they, respectively, favor a hexagonal polymorph along the 1D direction and possess a 2D layered crystal structure. Herein we demonstrate the construction of a 1D CdS nanowire/2D $ZnIn_2S_4$ nanosheet NHS and its shape evolution. Through an experimental and theoretical understanding into the bonding characteristics of the 1D/2D interface, we shall rationalize the evolution to the novel helical 1D/2D NHS.

The CdS nanowire/$ZnIn_2S_4$ nanosheet NHS (Figure 1 a) was synthesized in two steps. Initially, the CdS nanowires were obtained through a solvothermal method. Then, precursors of zinc, indium, and sulfur were introduced for secondary growth. $ZnIn_2S_4$ formed as perpendicular nanosheets (Figure 1 a) with a diameter of 20 nm and a thickness of less than 4 nm, and contained less than three layers of $ZnIn_2S_4$ molecules (one septuple layer: 1.23 nm; Supporting Information, Figure S2). This is the first example of a several-lattice-thick nanosheet grown onto a nanowire with defined orientation. The loading amount (the ratio of sulfur in $ZnIn_2S_4$ to that in CdS) could be tuned from 0 to 0.3. The element distribution was verified by Energy dispersive X-ray (EDX) element mapping (Figure S1 i). If this ratio further increased, the nanosheets would grow separately rather than onto the nanowire (Figure S1 c). This was probably due to the increased supersaturation of the precursors and homogeneous nucleation of $ZnIn_2S_4$ rather than its heterogeneous nucleation on CdS.[14] Without the CdS nanowire, $ZnIn_2S_4$ would also independently grow as ultrathin nanosheets with less than three layers (Figure S1 d). $ZnIn_2S_4$ belongs to the family of thiospinel structures (MIn_2S_4, M = Cd, Fe, Ni, Mn, among others).[25] Thus, we could also substitute Zn with other

[*] B. Xu, P. He, H. Liu, P. Wang, Prof. Dr. X. Wang
Department of Chemistry, Tsinghua University
Beijing, 100084 (China)
E-mail: wangxun@mail.tsinghua.edu.cn
Prof. Dr. G. Zhou
State Key Laboratory of Chemical Resource Engineering, Beijing University of Chemical Technology, Beijing, 100029 (China)

[**] This work was supported by NSFC (91127040, 21221062), and the State Key Project of Fundamental Research for Nanoscience and Nanotechnology (2011CB932402).

Supporting information for this article is available on the WWW under http://dx.doi.org/10.1002/anie.201310513.

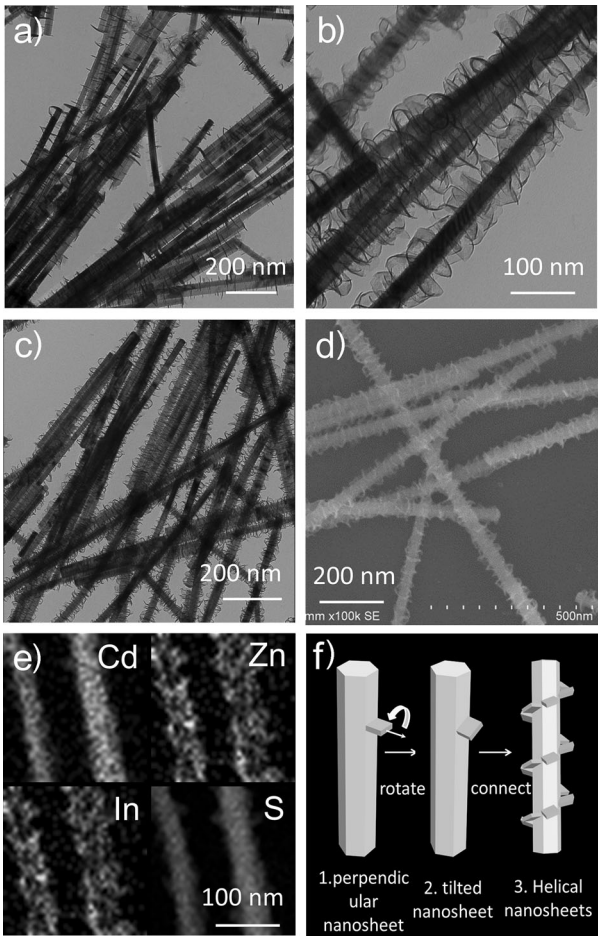

Figure 1. a) TEM image of the nanowire/nanosheet NHS. b–c) TEM images and d) SEM images of the nanowire/helical nanosheet NHS. e) EDX element mapping. f) The morphological evolution process.

metals (Cd, Fe, Ni, Mn) to obtain a series of 1D/2D NHSs (Figure S1e–h).

We emphasize that, as the reaction time was extended, the nanosheets would lean, exhibiting their basal planes in TEM analysis (Figure S1b). Based on the tilted 1D/2D NHS, additional precursors of Zn, In, and S were introduced in a third procedure. Helical and consecutive nanosheets were attached along the CdS nanowires (Figure 1b,c). Scanning Electron Microscopy (SEM) verified the stereo morphology (Figure 1d; see also Figure S3d). Helical inorganic nanostructures[26–30] mimicking helical biomolecules have been the focus of tremendous interest. To date, only 1D-1D features (core-shell or branched) have been found in inorganic helical NHSs.[27,29,30] 1D carbon nanotube/2D graphene nanoribbon helical structures were predicted by theoretical simulation,[31] but not experimentally realized. We have demonstrated here the first 1D nanowire/2D helical interconnected nanosheet NHSs.

As indicated by EDX element mapping (Figure 1e), Cd and S atoms were uniformly distributed in the wire, whereas Zn and In atoms were wrapped outside the wire. X-ray Diffraction (XRD) patterns (Figure S4) confirmed the hexagonal phase of the CdS nanowire (JCPDS No. 65-3414, space group: $P6_3mc$). For a single $ZnIn_2S_4$ nanosheet, the phase coincided with JCPDS No. 72-0773 (space group; $P6_3mc$), and the (002) and (006) reflection peaks were observed. As the $ZnIn_2S_4$ nanosheets in the NHSs are ultrathin, broadened peaks were merely observable until the loading ratio increased to 0.5. Raman spectra confirmed the crystal phases (Figure S6). X-ray photospectroscopy (XPS) peaks (Figure S5) corresponded well with previous reports (Supporting Information, Section 6). ICP-OES (Table S1) both confirmed the elemental composition.

To establish a deeper view of the 1D/2D interface at the atomic level, for better understanding of the formation mechanism, we first carried out various characterizations. SEM images revealed the hexagonal cross section of the CdS nanowire (Figure S3c). Through HRTEM, a fast Fourier transformation pattern (Figure 2a) indicated illumination by the electron beam along the [100] axis of a CdS nanowire with the lateral faces of {010}. As seen from Figure 2b, the CdS nanowire stretched along the [001] axis, parallel to the [001] axis of $ZnIn_2S_4$ that exposed its (006) planes in its two unconfined dimensions. The stability of 1D/2D NHS (Figure 1a) is an indication of perfect bonding between two units,

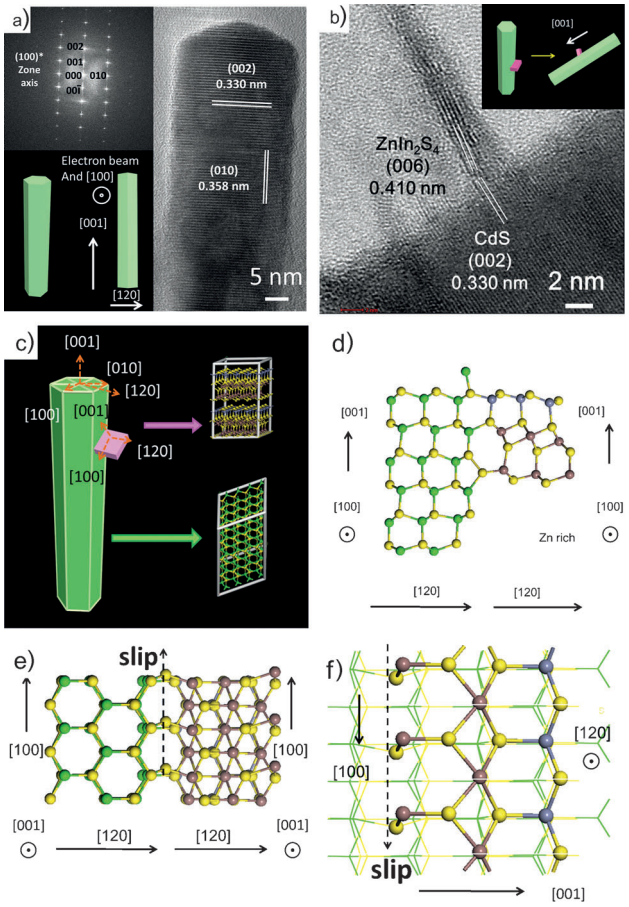

Figure 2. a) HRTEM image and the FFT pattern of a CdS nanowire. b) HRTEM image of a $ZnIn_2S_4$ nanosheet on a CdS nanowire. c) Model of the CdS-$ZnIn_2S_4$ NHS, d) The atom arrangement after DFT relaxation at the interface, as viewed along the [100] axis, e) the [001] axis, and f) the [120] axis, where a slip along the [100] axis is denoted. Cd green, S yellow, Zn blue, In brown.

requiring that the lateral face of the nanosheets fit the (010) surface of the nanowire to the greatest extent. The nucleation or formation of nanosheets on the nanowire can be viewed as the saturation of dangling bonds of (010) surface Cd and S atoms by Zn, In, and S atoms. In principle, the extent to which this process occurs is dependent upon the matches of dangling bonds and lattice between 1D and 2D units. The former (chemical or electronic effects) ensures as strong a bonding as possible between the two units, whereas the later (geometrical effects) allows as little deformation energy as possible for the two units. Further taking into account that the two units belong to the same space group ($P6_3mc$; Figure 2c), we cut several typical lateral faces from 2D $ZnIn_2S_4$ nanosheets (Figure S7a,b) and compared them with the (010) surface of CdS (Figure S7c). Following the lattice and dangling bond matches, we affirm that the most preferable bonding lateral face of the $ZnIn_2S_4$ nanosheet is the {010} one, which has Zn-S_1-S_2 and In-S_1-S_2 terminals, respectively; these correspond to two different 1D/2D interfaces, but hold a similar bonding mode (Figure 2c,d; see also Figure S7d). More precisely, density functional theory (DFT) calculations were undertaken and indicated new bonds (Zn/In-S_{NW}, S_1-Cd_1, S_2-Cd_2 and S_2-S'_{NW} in Figure S7d) at the interface. Taking the Zn-S_1-S_2 terminal binding to the nanowire as an example (note that the conclusions drawn could be extended to the In-S_1-S_2 terminal): The unique layered structure of $ZnIn_2S_4$ nanosheets (separated Zn/In-layers are central symmetric with respect to In atoms in the middle layer, as seen in Figure S2) determines different binding modes at the Zn-layer and In-layer. This bonding characteristic certainly will allow their different stresses forced and lattice deformations. DFT calculations reveal that, relative to Zn and S_1, the S_2 in the In layer is pronouncedly deviated in the [100] direction (Figure 2e,f). The slip of surface S_2 layer with respect to other parts, such as a screw dislocation pinned at the interface,[32] produces a lattice twist in 2D nanosheets and a shear along the [100] direction (Figure 2e,f). In summary, besides the lattice mismatch, the bond mismatch allows the $ZnIn_2S_4$ nanosheets to rotate along the ⟨120⟩ axis (Figure S10a), which is in agreement with the experimental results (TEM images) after 12 h reaction time (Figure S1b). This tilt or rotation phenomenon is common in epitaxy between two compounds with large misfit.[33]

As indicated by the layered crystal structure of $ZnIn_2S_4$ (Figure S2), the {002} surfaces of $ZnIn_2S_4$ nanosheets are negatively charged with dipole moments (Supporting Information, Section 8-2). A second nanosheet growing in is repulsed by an already present one. Moreover, the stress on the nanowire induced by the 1D/2D mismatches will restrict the growth of new nanosheets in the nearby area. Consequently, along the [001] axis, the nanosheets are separated at some distance, corresponding well with TEM data (Figure 1a and S1b).

In the third procedure, the newly grown $ZnIn_2S_4$ nanosheets would fill the void space of the old nanosheets along the unconfined two dimensions. Subsequently, separate $ZnIn_2S_4$ nanosheets connect each other, forming helical and continuous nanosheets (Figure 1b). To propose a tentative mechanism on this shape evolution, we scrutinize the various energies which were balanced in this process, step by step. First, starting from a single CdS nanowire, the growth of $ZnIn_2S_4$ nanosheet onto it leads to energy stabilization through the formation of a new interface. Then, we could look into the initial stage when the first and the second sheet were grown on the nanowire and the Columbic repulsion was introduced (Figures S10c and S8; see also the Supporting Information, Section 8-2). Finally we focused on one group of the six old $ZnIn_2S_4$ nanosheets (pink) that were bound around the six {010} surfaces of a CdS nanowire, and the connection between them by newly grown sheets (light green), which induce a surface-energy decrease (Figure S10b). The sum of the interface energy, electrostatic energy, and surface energy (Supporting Information, Section 8-3) leads to the conclusion that the most energy-favorable case is that all six nanosheets rotate counterclockwise. Further connection between translational equivalent groups of nanosheets along the [001] axis results in the long-range helical suprastructure (Figure S10d).

To date, the growth of inorganic helical structures has been proposed to proceed through templates[26,28] or rotary defects, such as screw-dislocation.[27,29,30] We found here that the rotation of 2D sheets on a 1D wire, which originated from the lattice mismatch, might be combinatorially utilized to construct helical 1D/2D NHSs, based on the proper choice of a layered material and another 1D material with the same space group and similar coordination environment, but mismatched lattice parameters.

CdS and $ZnIn_2S_4$ are both excellent candidates as the anode materials in the photoelectrochemical cells (PECs) where S^{2-} is used as the sacrificing reagent.[34] The single components and their mixed counterparts all performed moderately in PECs (Figure 3a,b). However, after 0.1 molar ratio $Zn_{0.25}In_{0.5}S$ nanosheets were grown onto the CdS nanowires, the photocurrent increased to about 2 mA, which is three times that of a single CdS nanowire (Figure 3a). Furthermore, the best performance (7 mA) was achieved with a 1 CdS/0.5 $Zn_{0.25}In_{0.5}S$ nanowire/helical nanosheet NHS,

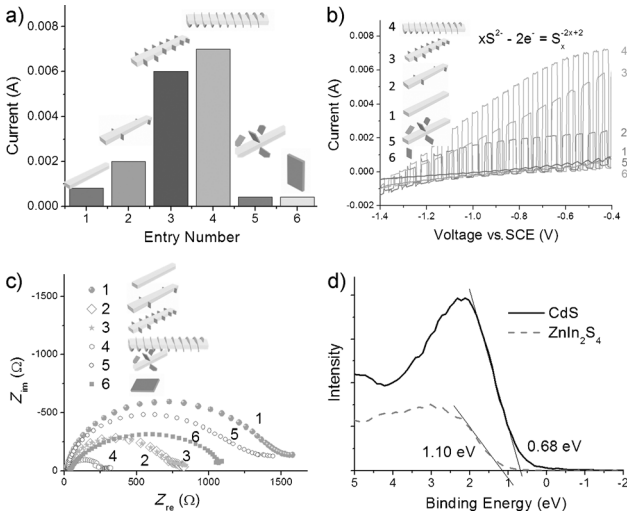

Figure 3. a) Comparison of photocurrents. b) *i-V* scans of samples 1–6. c) EIS spectra of samples 1–6. d) XPS valence-band spectra of samples 1–6.

which was more than ten times that of the single units (Figure 3a).

The greatly enhanced performance of the NHSs may originate from the 1D/2D interface that facilitated the charge separation and transport.[35] The assumption was verified by the experimental results that the NHSs had smaller electrochemical impedances than individual nanowires, nanosheets, and a mixture of the two (Figure 3c; see also the Supporting Information, Section 10).[35] Combing the result of XPS valence spectra (Figure 3d) and the band-gap values extrapolated by UV/Vis spectra (Figure S11a),[22] we deduced the band alignments of the NHS (Figure 4a; see also the Supporting Information, Section 11). By virtue of this straddling band feature of the NHS, electrons would migrate from $ZnIn_2S_4$ to CdS, and holes would be transported in the opposite direction at the interface (Figure 4a).[35] Compared with bulk $ZnIn_2S_4$, the atomically thick $ZnIn_2S_4$ nanosheet might possess a higher conduction band minimum (CBM) and a lower valence band maximum (VBM), which might induce a smaller VBM offset between $ZnIn_2S_4$ and CdS, thus facilitating the injection of holes from the VBM of CdS. The above analysis was further verified by a Mott–Schottky plot that derived the increased charge carrier density after the construction of the 1D/2D interface[36] (Supporting Information, Section 12).

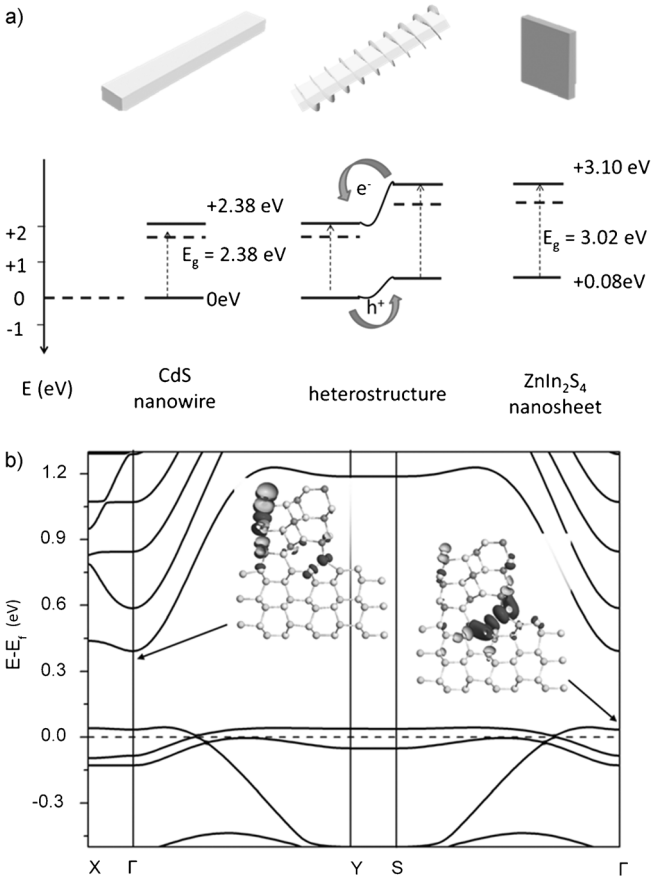

Figure 4. a) The band alignment and b) band structure of the nano-heterostructure. The Fermi energy (E_F) is set to zero. Insets: Isosurface plots of the squared wave function at the Γ point of the bands in the gap. The isovalue is 0.006 e Å^3.

DFT calculations further supported the experimental results. The calculated electronic structures revealed that new bands near VBM and CBM in the gap are mainly contributed to by the p orbitals of the interface atoms, especially the S atoms (Figure 4b). These interface states offer a few carrier transport channels for the electron/hole transfer between the 1D nanowires and the 2D nanosheets, which is in agreement with the band alignment. Accumulated holes and the exposure of almost an entire surface in the 2D unit allowed the 1D/2D NHS to have many more reaction sites for the anode reaction, as compared to the individual components.

As an advanced form of 1D/2D NHS with a continuous 1D/2D interface, the enhanced performance of the nanowire/helical nanosheet structure versus its simple nanowire/nanosheet counterpart might stem from the following aspects: 1) The more abundant interfaces between CdS and $ZnIn_2S_4$ facilitate charge separation, and in the continuous interface the charge carriers are delocalized and the transport is more favorable. 2) The connected nanosheets act as efficient light-scattering units and better capture light.[19] More appealingly, with its chirality, this helical structure is also a potential candidate in polarized-light optoelectronic applications.

In conclusion, we have demonstrated the synthesis of 1D CdS/2D $ZnIn_2S_4$ NHS and its morphological transformation to 1D/2D helical NHS. It was proposed that the lattice-mismatch-induced rotation of the nanosheets was critical for this process. The helical structure was the best-performing one in PECs, owing to the modulated band alignment. As we have demonstrated the insights into the shape-evolution mechanism and the electronic structures of these NHSs, we hope this contribution will shed light on the rational design of more complex 1D/2D NHSs with accompanying applications in solar energy conversion and other fields.

Received: December 4, 2013
Published online: January 29, 2014

Keywords: helical structures · heterostructures · interfaces · nanostructures · photoanodes

[1] L. Brus, *J. Phys. Chem.* **1986**, *90*, 2555.
[2] S. Iijima, *Nature* **1991**, *354*, 56.
[3] T. J. Trentler, K. M. Hickman, S. C. Goel, A. M. Viano, P. C. Gibbons, W. E. Buhro, *Science* **1995**, *270*, 1791.
[4] A. M. Morales, C. M. Lieber, *Science* **1998**, *279*, 208.
[5] M. H. Huang, S. Mao, H. Feick, H. Yan, Y. Wu, H. Kind, E. Weber, R. Russo, P. Yang, *Science* **2001**, *292*, 1897.
[6] Z. W. Pan, Z. R. Dai, Z. L. Wang, *Science* **2001**, *291*, 1947.
[7] Y. Gao, Y. Bando, *Nature* **2002**, *415*, 599.
[8] M. Heurlin, M. H. Magnusson, D. Lindgren, M. Ek, L. R. Wallenberg, K. Deppert, L. Samuelson, *Nature* **2012**, *492*, 90.
[9] K. S. Novoselov, A. K. Geim, S. V. Morozov, D. Jiang, Y. Zhang, S. V. Dubonos, I. V. Grigorieva, A. A. Firsov, *Science* **2004**, *306*, 666.
[10] K. P. Loh, Q. Bao, G. Eda, M. Chhowalla, *Nat. Chem.* **2010**, *2*, 1015.
[11] S. Z. Butler, et al., *ACS Nano* **2013**, *7*, 2898.

[12] M. Chhowalla, H. S. Shin, G. Eda, L.-J. Li, K. P. Loh, H. Zhang, *Nat. Chem.* **2013**, *5*, 263.
[13] C. Li, Y. Yu, M. Chi, L. Cao, *Nano Lett.* **2013**, *13*, 948.
[14] R. Costi, A. E. Saunders, U. Banin, *Angew. Chem.* **2010**, *122*, 4996; *Angew. Chem. Int. Ed.* **2010**, *49*, 4878.
[15] J. Liu, J. Jiang, C. Cheng, H. Li, J. Zhang, H. Gong, H. J. Fan, *Adv. Mater.* **2011**, *23*, 2076.
[16] W. Zhou, X. Cao, Z. Zeng, W. Shi, Y. Zhu, Q. Yan, H. Liu, J. Wang, H. Zhang, *Energy Environ. Sci.* **2013**, *6*, 2216.
[17] W. Wang, J. Goebl, L. He, S. Aloni, Y. Hu, L. Zhen, Y. Yin, *J. Am. Chem. Soc.* **2010**, *132*, 17316.
[18] G. Zhang, H. Fang, H. Yang, L. A. Jauregui, Y. P. Chen, Y. Wu, *Nano Lett.* **2012**, *12*, 3627.
[19] M. J. Bierman, S. Jin, *Energy Environ. Sci.* **2009**, *2*, 1050.
[20] A. I. Hochbaum, P. Yang, *Chem. Rev.* **2010**, *110*, 527.
[21] S. Yang, Y. Gong, J. Zhang, L. Zhan, L. Ma, Z. Fang, R. Vajtai, X. Wang, P. M. Ajayan, *Adv. Mater.* **2013**, *25*, 2452.
[22] M. Guan, C. Xiao, J. Zhang, S. Fan, R. An, Q. Cheng, J. Xie, M. Zhou, B. Ye, Y. Xie, *J. Am. Chem. Soc.* **2013**, *135*, 10411.
[23] H. Li, X. Wang, J. Xu, Q. Zhang, Y. Bando, D. Golberg, Y. Ma, T. Zhai, *Adv. Mater.* **2013**, *25*, 3017.
[24] Z. Lei, W. You, M. Liu, G. Zhou, T. Takata, M. Hara, K. Domen, C. Li, *Chem. Commun.* **2003**, 2142.
[25] M. A. Sriram, P. H. McMichael, A. Waghray, P. N. Kumta, S. Misture, X. L. Wang, *J. Mater. Sci.* **1998**, *33*, 4333.
[26] J. H. Jung, Y. Ono, K. Hanabusa, S. Shinkai, *J. Am. Chem. Soc.* **2000**, *122*, 5008.
[27] H.-F. Zhang, C.-M. Wang, L.-S. Wang, *Nano Lett.* **2002**, *2*, 941.
[28] E. D. Sone, E. R. Zubarev, S. I. Stupp, *Angew. Chem.* **2002**, *114*, 1781; *Angew. Chem. Int. Ed.* **2002**, *41*, 1705.
[29] M. J. Bierman, Y. K. A. Lau, A. V. Kvit, A. L. Schmitt, S. Jin, *Science* **2008**, *320*, 1060.
[30] J. Zhu, H. Peng, A. F. Marshall, D. M. Barnett, W. D. Nix, Y. Cui, *Nat. Nanotechnol.* **2008**, *3*, 477.
[31] N. Patra, Y. Song, P. Král, *ACS Nano* **2011**, *5*, 1798.
[32] C. Kittel, *Introduction to Solid State Physics*, 8th ed., Wiley, Hoboken, **2005**, pp. 603 – 604.
[33] A. Zur, T. C. McGill, *J. Appl. Phys.* **1984**, *55*, 378.
[34] A. B. Ellis, S. W. Kaiser, M. S. Wrighton, *J. Am. Chem. Soc.* **1976**, *98*, 6855.
[35] E. S. Kim, N. Nishimura, G. Magesh, J. Y. Kim, J.-W. Jang, H. Jun, J. Kubota, K. Domen, J. S. Lee, *J. Am. Chem. Soc.* **2013**, *135*, 5375.
[36] M. Ye, J. Gong, Y. Lai, C. Lin, Z. Lin, *J. Am. Chem. Soc.* **2012**, *134*, 15720.

